Original Article

Enhanced Structural, Morphological and Optical Features of Ti_x MnNiO (X= 1, 2, and 3 mL) Synthesized Using Hydrothermal Approach

Azmat Hussain[1,2] | Saira Habib[1,2] | Inam Ullah[1,2] | Fahma Sahreen[1,3] | Imtiaz Ahmad[1,4] | Imosobomeh L. Ikhioya[1,5*]

[1]National Centre for Physics, Quaid-i-Azam University Campus, Islamabad, 44000, Pakistan
[2]Department of Physics, Hazara University Mansehra, Pakistan
[3]Department of Physics, School of Natural Science (SNS), National University of Sciences & Technology (NUST), H-12, Islamabad, Pakistan
[4]Department of Physics, University of Engineering and Technology Lahore, Pakistan
[5]Department of Physics and Astronomy, University of Nigeria, Nsukka, 410001, Nigeria

Use your device to scan and read the article online

Citation A. Hussain, S. Habib, I. Ullah, F. Sahreen, I. Ahmad, I. L. Ikhioya, **Enhanced Structural, Morphological and Optical Features of Ti_x MnNiO (X= 1, 2, and 3 mL) Synthesized Using Hydrothermal Approach.** *Eurasian J. Sci. Technol.,* **2024**, *4*(3), 195-207.

https://doi.org/10.48309/EJST.2024.428429.1117

Article info:
Received: 2023-12-03
Accepted: 2024-01-03
Available Online: 2024-01-28
ID: EJST-2312-1117
Checked for Plagiarism: Yes
Checked Language: Yes

Keywords:
Hydrothermal, Titanium, MnNiO, Bandgap, Photovoltaic.

ABSTRACT

In this study, a hydrothermal method was used to synthesize Tix MnNiO nanostructures for photovoltaic applications. The synthesized films display a hexagonal phase and are polycrystalline. They exhibit a preferred alignment on the (111), (112), (116), (121), and (200) planes. The angles 2 theta are (26.612, 30.816, 32.154, 33.154, and 37.856) degrees. The structural properties of the material are enhanced by incorporating titanium into the lattice of manganese, nickel oxide. By integrating titanium into the MnNiO lattice, the material's UV absorbance was enhanced. At 310 nm, the noticeable peaks of the materials show a rise in titanium concentration, leading to enhanced absorbance during synthesis. The material absorbance decreases as the wavelength of light in the visible region increases. The indirect bandgap energy of the synthesized Tix MnNiO film decreases with increasing molar concentration, ranging from 2.75 eV to 1.82-1.50 eV.

***Corresponding Author: Imosobomeh L. Ikhioya,** imosobomeh.ikhioya@unn.edu.ng*

Introduction

The growing demand for energy is shifting focus to renewable technologies because of the rapid consumption of fossil fuels [1-3]. Nanomaterials possess remarkable cycling stability, high-power density, and excellent reversibility, making them ideal for energy-storage applications. Nanomaterials play a crucial role in portable electronic products, electric vehicles, and industrial power supplies. Nanotechnology combines knowledge from various fields to make scientific advancements [4,5]. It has uses in medicine, biofuel production, wastewater management, and drug delivery. Various technologies utilize nanoscale materials, including pharmaceuticals, cosmetics, and catalysis/photocatalysis. Nanotechnology is based on the use of nanoparticles as fundamental building blocks. Synthesis of metal nanomaterials with exact shape and size was achieved for catalysis and biomedicine. Nanomaterials comprise nanoparticles that are 100 nm or smaller [6-12]. Nanoparticles can range in size from 1 to 100 nm. Nanoparticles were used in electronics and biofuel production because of their small size. The nanomaterials functionality is enhanced by factors like physical properties and an increased surface to volume ratio [14,15]. The hydrothermal method allows for composition control of materials via multiphase reactions. The synthesis route is straightforward, manageable, fast, and affordable, producing nanomaterials with low vapor pressure and minimal material loss.

The attention on opting for electrode materials with outstanding electrochemical performance has intensified, because electrode materials mainly limit the specific capacitance and energy density of nanomaterials [16,17]. Electric double-layer capacitors often use activated carbon, porous carbon, carbon nanotubes, and graphene as electrodes. Transition metal oxides such as V_2O_5, MnO_2, RuO_2, and as well as hydroxides like $Co(OH)_2$ and $Ni(OH)_2$, are notable examples. There are countless. They are often used. Researchers have extensively studied high-capacitance pseudo-capacitive materials, including conductive polymers. Despite this, particular transition metal hydroxides such as $Co(OH)_2$ and $Ni(OH)_2$ demonstrate properties resembling those of batteries [18-20]. The range of oxidation states and superior electrochemical performance make ternary transition metal oxides valuable over binary oxides. Researchers have extensively studied $NiCo_2O_2$ and $CoMo_2O_2$ as electrode materials for supercapacitors with a spinel structure. The economic and technical impact of replacing Co with Cu and Mn in alternative spinel materials is expected to be significant, considering the high cost of Co and the necessity for improved electrochemical performance. The capacitive behavior of Ni-Mn based oxides has resulted in widespread research. $NiMnO_3$, which has an ilmenite structure, has not received the same level of research as its well-known counterparts, such as $NiMn_2O_4$, which are extensively studied as electrode materials for supercapacitors [21-23].

A significant technology challenge in the 21st century is the replacement of fossil fuels with renewable energy for humanity. There is hope for achieving energy sustainability through recent advancements in PV solar cell technology. Modern solar panels are inefficient and costly by large-scale power grids. The major determinant for large-scale power generation of any PV solar technology is cost [19]. Technological advancements offer numerous possibilities for tackling the worldwide energy crisis. Metal oxide-based solar cells have significantly advanced PV technology. Nanomaterials such as MnNiO, nanowires, or quantum dots could enhance the efficiency of PV cells [24-29]. The concern is significant about reducing manufacturing costs through the use of affordable nanostructured materials and processes.

A composite of $MnNiO_3/Ni_6MnO_8$ was synthesized by Guo *et al.* [30] through

hydrothermal conditions at 120-160 °C with different growth times. The $MnNiO_3/Ni_6MnO_8$ nanospheres with a flower-like 3D structure was successfully synthesized at 140 °C for 10 hours. The $MnNiO_3/Ni_6MnO_8$ structure, with its unique 3D spherical shape and mesopores, enhances electrolyte ion transport and increases redox active sites. The energy storage mechanism of $MnNiO_3/Ni_6MnO_8$ is examined, revealing its dominance as a diffusion-controlled process in battery-type electrode material. The $MnNiO_3/Ni_6MnO_8$ nanospheres prepared in this way are also used for constructing a hybrid device. At a specific power of 1074.7, the device can provide a specific energy of 22.3 Wh/kg. The $MnNiO_3/Ni_6MnO_8$/AC device can successfully light up commercial LEDs of different colors, demonstrating the promising application potential of the $MnNiO_3/Ni_6MnO_8$ electrode.

Hydrothermal synthesis is a process that crystallizes substances in a sealed container from their high-temperature aqueous solution [13]. This technique produces a greater amount of crystalline material compared to other methods. The preparation of distinctive titanium-manganese, nickel oxide (Ti_x MnNiO) nanostructures involves hydrothermal treatment. The material melting point may lead to the creation of unstable crystal phases. As far as we know, the hydrothermal approach has not been employed to synthesize titanium with MnNiO material.

Titanium-manganese, nickel oxide (Tix MnNiO) nanostructures material was synthesized using a hydrothermal approach in this study for photovoltaic application. Various characterization equipment's will be used to conduct structural, elemental, optical, and visible analysis of the material.

Experimental

Materials

The study involves these materials: titanium tetrachloride ($TiCl_4$), manganese (II) nitrate hexahydrate ($Mn(NO_3)_2{\cdot}6H_2O$) Sigma-Aldrich 98%, nickel (II) nitrate hexahydrate. $Ni(NO_3)_2{\cdot}6H_2O$ Sigma-Aldrich 99%, potassium hydroxide (KOH), α-terpineol, polyethylene glycol, FTO-substrate, deionized water, heating mantle, an oven that has a temperature range of 50 to 1000 °C.

Synthesis of Tix MnNiO (X= 1, 2, and 3 mL)

A 0.2 M of Manganese (II) nitrate hexahydrate ($Mn(NO_3)_2{\cdot}6H_2O$), nickel (II) nitrate hexahydrate $Ni(NO_3)_2{\cdot}6H_2O$ and potassium hydroxide (KOH) were used to synthesize Ti_x MnNiO (X= 1, 2, and 3 mL**)**. 20 mL of potassium hydroxide with titanium tetrachloride ($TiCl_4$) at (1-3) mL was stirred for 40 minutes at room temperature. To achieve a consistent solution, a mixture of 0.5 g of α-terpineol, polyethylene glycol, and other solutions was stirred for 45 minutes at room temperature. For hydrothermal processing, the FTO glass and solution were placed in a stainless-steel autoclave lined with Teflon. The temperature of the solution stayed at 200 °C for of 7 hours. After cooling down naturally to room temperature, the deposited Tix MnNiO (X= 1, 2, and 3 mL) on FTO substrate was vacuum-dried at 70 °C for 40 minutes, as displayed in Figure 1. The films were analyzed using different techniques to determine their optical, electrical, structural, morphological, and elemental compositions. Structural and elemental compositions were analyzed using the NPUFEI-NNS45 SEM. The absorbance wavelength of the films was measured using a 756S UV-Visible spectrophotometer between 300 to 1000 nm. The electrical properties of the films were analyzed using the Jandel four-point probes method.

Results

Optical study of Tix MnNiO (X= 1, 2, and 3 mL)

The optical properties of Tix MnNiO (X= 1, 2, and 3 mL) synthesized through hydrothermal process were analyzed using a visible spectrophotometer (300 to 1000 nm), as shown in Figure 2. Incorporating titanium

into the lattice of MnNiO improved the material's absorbance in the UV region of the spectra, as demonstrated in Figure 2 (H1). The materials' prominent peaks become apparent at 310 nm, indicating a rise in titanium concentration during synthesis and boosting material absorbance. The material absorbance decreases as the wavelength of light radiation at the visible region increases. The greater amount of titanium results in the highest absorbance in the spectra and increasing the film concentration improves all optical properties. Harnessing energy from the sun requires vital synthesized materials. Hydrothermally synthesized Tix MnNiO (X=1, 2, and 3 mL) is crucial for photovoltaic and solar cell applications. The material absorbs at a higher rate with a higher concentration of titanium. Introducing titanium may have led to a larger crystallite size, as indicated by the increase in the observed crystallite peak in the XRD pattern. A larger crystallite size can cause a higher specific surface area and increased optical absorbance. The films have excellent absorbency, making them perfect for solar cell and energy production.

At 310 nm, Figure 2 (H_2) shows an exceptionally high transmittance rate, exceeding 100%. Tix MnNiO (X=1, 2, and 3 mL) exhibits an increase in transmittance in the infrared spectral range for all materials. As the concentration of titanium increases, the transmittance spectra decrease. The films displayed a drop in electrical resistivity, implying it could potentially be the reason. A higher specific surface area may be achieved by decreasing the film thickness, which could improve optical transmittance. Because of their high transmittance rate, these films are ideal for solar cell systems photovoltaics, and energy production. The highest reflectance was observed in the UV region, as illustrated in Figure 2 (H_3). The evaluation showed that the films had low reflectance in both regions, making them perfect for solar and photovoltaic cells. The low reflectance of the material is caused by light interacting with its surface and canceling out reflected light waves. Overestimating the material's optical thickness results in their occurrence. The earlier estimate may not fully consider larger-than-expected errors in surface reflectance. The influence of adjacency effects and persistent residuals explains this primarily. Figure 2 (H4) illustrates the energy bandgap representation of Tix MnNiO (X=1, 2, and 3 mL) through the $(\alpha hv)^2$ against hv plot. The graph helped determine the indirect bandgap of the films. The indirect bandgap energy of the synthesized Tix MnNiO (X=1, 2, and 3 mL) film decreases as the molar concentration of the material increases, shifting from 2.75 eV to a

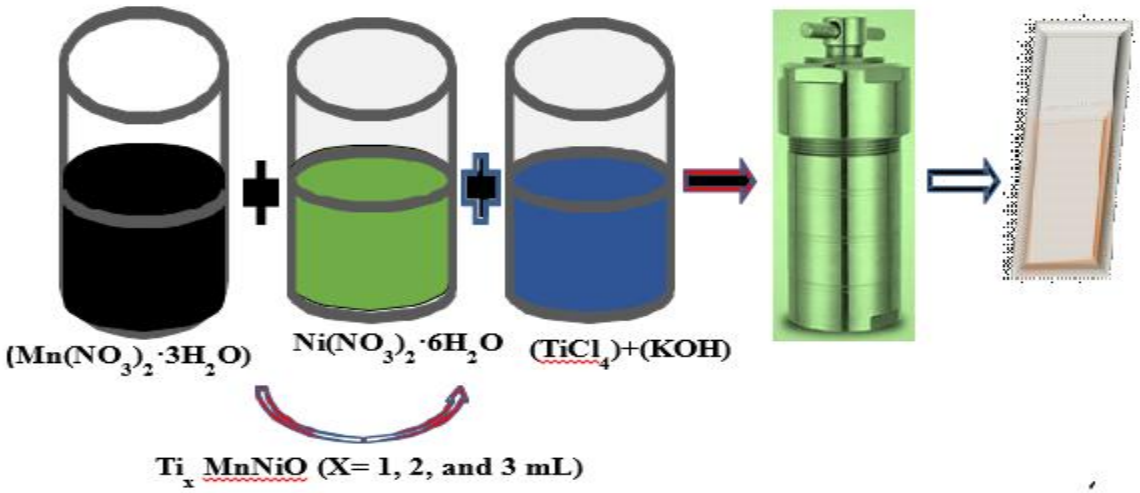

Figure 1 Schematic diagram illustrating the synthesis procedure

range of 1.82–1.50 eV. Figure 3 (H5) displays the refractive index of the synthesized material. The plot shows that the refractive index increases as titanium concentration increases, reaching a maximum value before sharply decreasing with MnNiO with the lowest refractive index. The extinction coefficient of Tix MnNiO (X=1, 2, and 3 mL) is inidicated in Figure 3 (H6). The material with the highest concentration of titanium showed the highest extinction coefficient value. The real dielectric constant of Tix MnNiO (X=1, 2, and 3 mL) increases with higher titanium concentration, peaks between 2.5-3.5 eV, and then decreases at higher photon energy (Figure 3, H7 and H8). The dielectric constant of the deposited films increases as the titanium concentration rises.

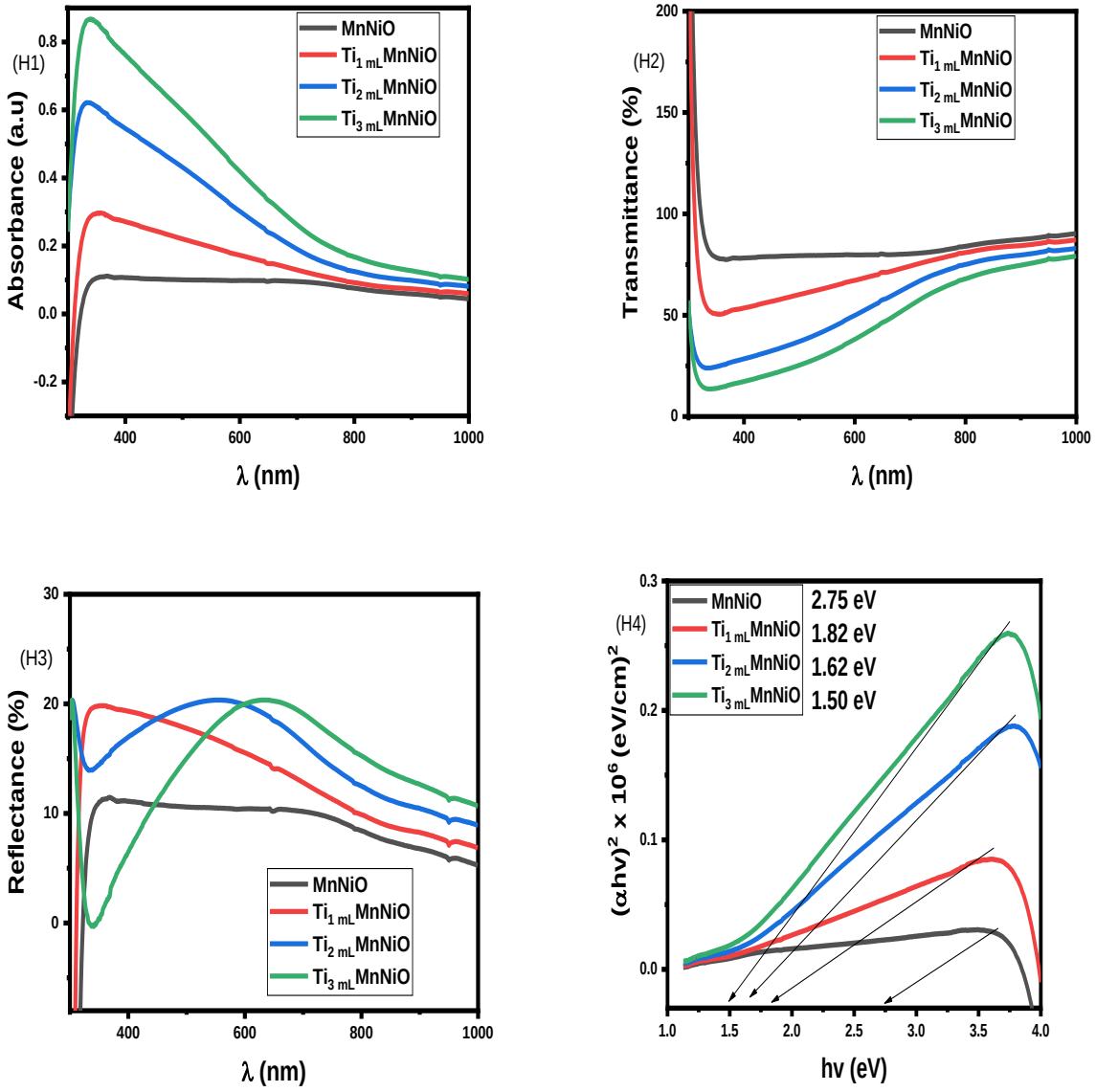

Figure 2 (H1) absorbance, (H2) transmittance, (H3) reflectance, and (H4) bandgap energy

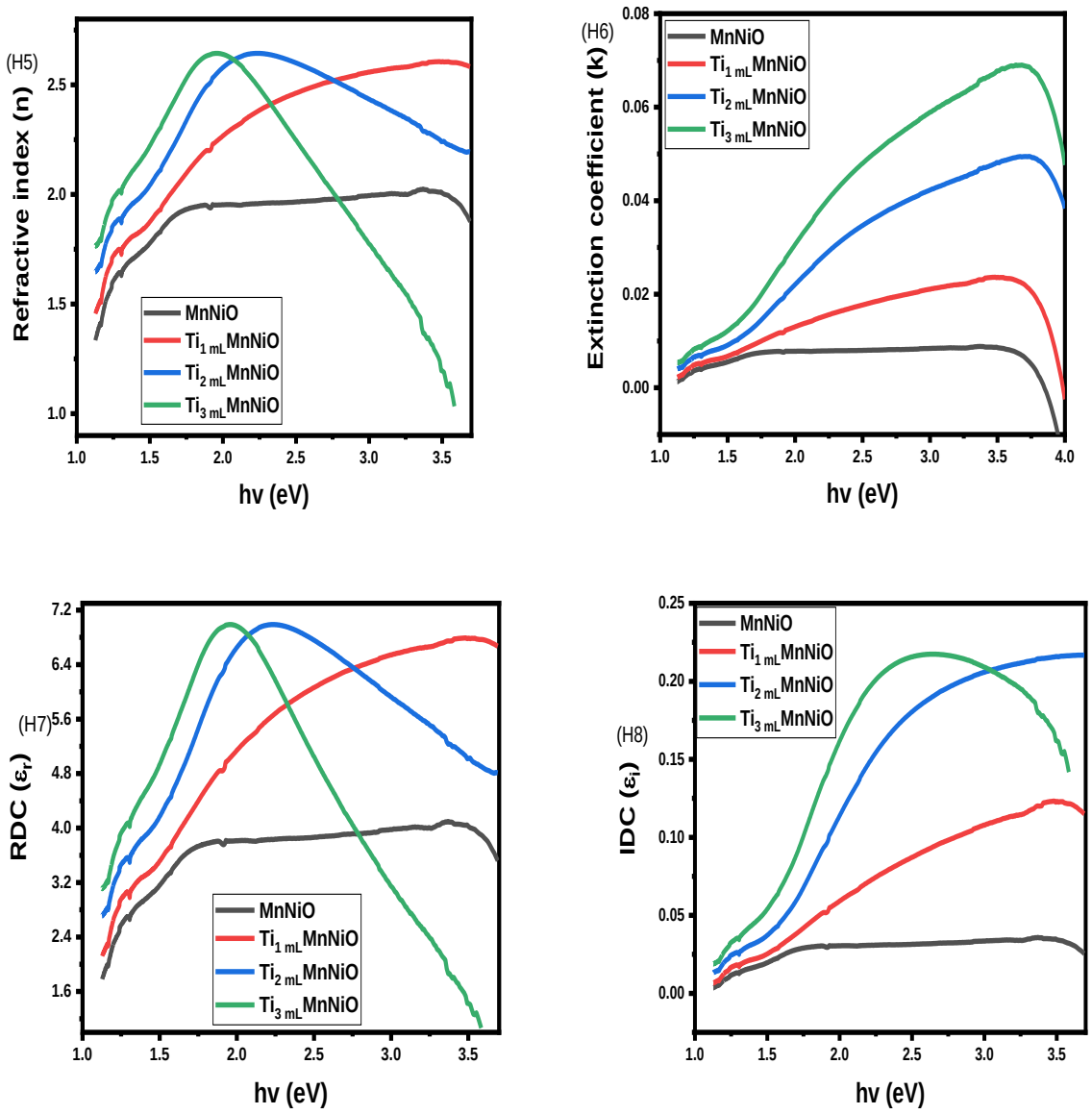

Figure 3 (H5) refractive index, (H6) extinction coefficient, (H7) real, and (H4) imaginary dielectric constant

XRD analysis of Tix MnNiO (X=1, 2, and 3 mL)

The XRD result of Tix MnNiO materials with different X values (1, 2, and 3 mL) is shown in Figure 4. The synthesized films exhibit a hexagonal phase and are polycrystalline, with a preferred orientation along the (111), (112), (116), (121), and (200) planes [31,32]. The corresponding 2 theta angles are (26.612, 30.816, 32.154, 33.154, and 37.856) degrees. The structural properties of the material are improved by incorporating titanium into the lattice of manganese, nickel oxide. Equations (1-4) were utilized to approximate the structural characteristics in Table 1.

$$D = \frac{k\lambda}{\cos\theta} \quad (1)$$

$$d = \frac{\lambda}{2\sin\theta} \quad (2)$$

$$\delta = \frac{1}{D} \quad (3)$$

$$a = d\sqrt{h^2 + k^2 + l^2} \quad (4)$$

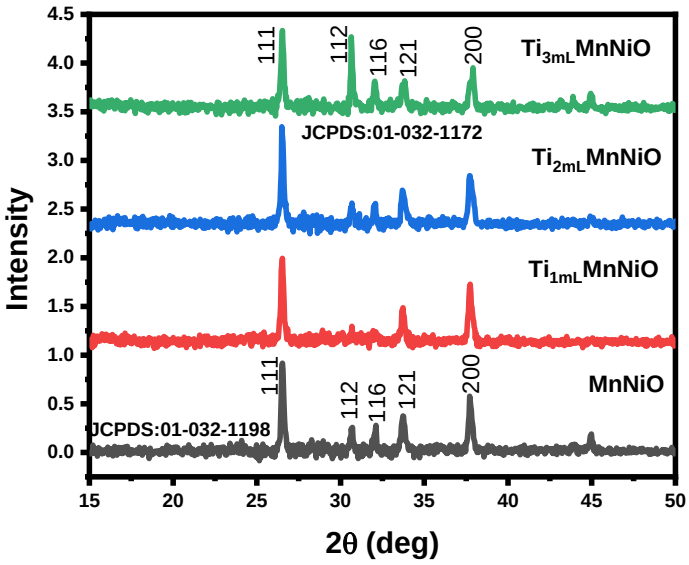

Figure 4 XRD pattern of Tix MnNiO (X=1, 2, and 3 mL)

Table 1 Structural properties of Tix MnNiO (X=1, 2, and 3 mL)

Films	2θ (deg.)	d (spacing) Å	a (Å)	(β)	(hkl)	(D) nm	σ lines/m² X 10¹⁸
MnNiO	26.536	3.358	5.817	0.9234	111	1.543	1.277
	30.716	2.910	5.820	0.9243	112	1.556	1.256
	32.115	2.786	5.573	0.9245	116	1.561	1.248
	33.714	2.658	5.942	0.9252	121	1.567	1.240
	37.787	2.380	5.830	0.9256	200	1.584	1.213
Ti 1 mLMnNiO	26.612	3.349	5.800	0.7367	111	1.925	8.133
	30.816	2.901	5.802	0.7369	112	1.953	7.988
	32.154	2.783	5.866	0.7371	116	1.959	7.937
	33.154	2.648	5.922	0.7374	121	1.966	7.879
	37.856	2.376	5.820	0.7376	200	1.988	7.704
Ti 2 mLMnNiO	26.612	3.349	5.800	0.7255	111	1.965	7.888
	30.816	2.901	5.802	0.7257	112	1.983	7.747
	32.154	2.783	5.866	0.7260	116	1.989	7.700
	33.154	2.648	5.922	0.7264	121	1.996	7.645
	37.856	2.376	5.820	0.7268	200	2.018	7.480
Ti 3 mLMnNiO	26.612	3.349	5.800	0.7564	111	1.885	8.574
	30.816	2.901	5.802	0.7569	112	1.901	8.427
	32.154	2.783	5.866	0.7575	116	1.906	8.383
	33.154	2.648	5.922	0.7579	121	1.913	8.323
	37.856	2.376	5.820	0.7582	200	1.934	8.140

Surface micrograph of Tix MnNiO (X=1, 2, and 3 mL)

The surface micrograph of Tix MnNiO (X=1, 2, and 3 mL) is demonstrated in Figure 5. The films have a noticeable nano structure, with a visible pebble-like material. Incorporating titanium into the MnNiO lattice causes a decrease in nanoparticle size. The high concentration of titanium led to an increase in the surface energy of the material, resulting in the presence of nonflake clusters on the film's surface. The nanoparticle's susceptibility to agglomeration increased because of a higher concentration of titanium. Due to strain, the lattice experienced a change in orientation, leading to the formation of a dislocation near the surface. The lattice strain aligns with the observed strain in their structural property. Figure 6 displays the elemental composition of Tix MnNiO for X values of 1, 2, and 3 mL. The spectrum displays all the elements needed for Tix MnNiO formation (X=1, 2, and 3 mL). It is possible that the composition of the FTO substrate used during synthesis is the other observed element.

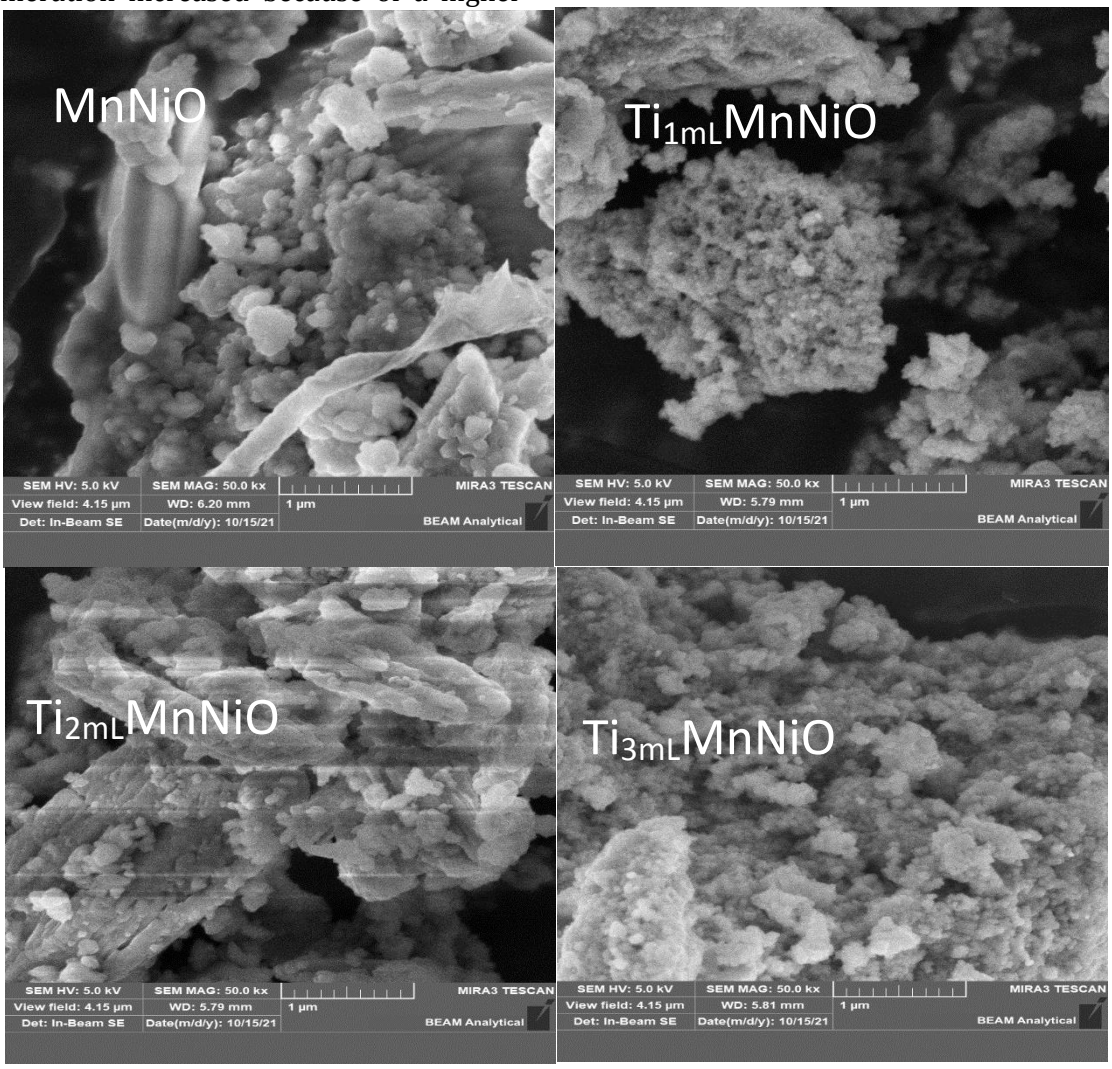

Figure 5 SEM analysis of the material

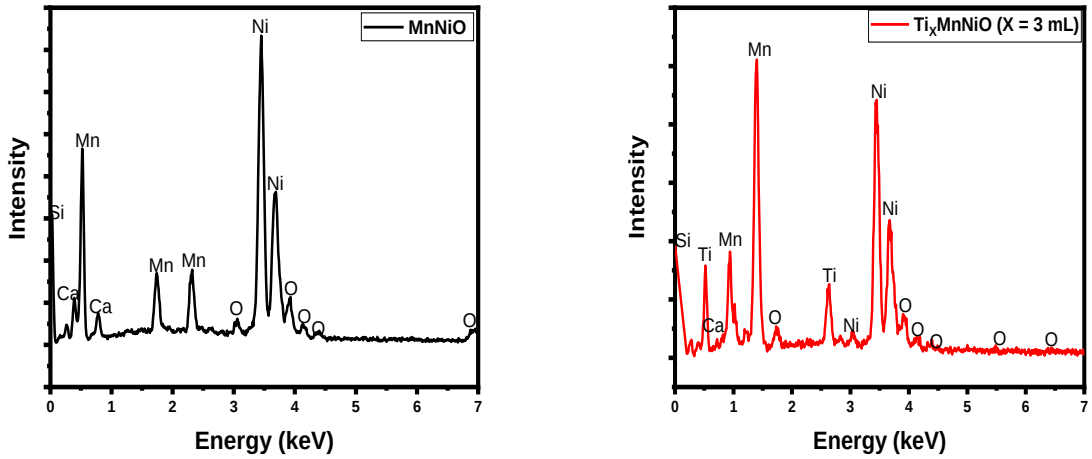

Figure 6 Material's energy dispersive X-ray analysis

Investigation of the electrical properties of Tix MnNiO (X=1, 2, and 3 mL)

Film thickness, resistivity, and conductivity are correlated, as shown in Figure 7. Decreasing material thickness leads to increased films conductivity and decreased resistivity. The alignment occurs because higher titanium concentration increases carrier concentration, enhancing the material's conductivity. The material's capacity for handling increased current is helpful in photovoltaic applications. Table 2 provides valuable insights into the photovoltaic properties of Tix MnNiO (X=1, 2, and 3 mL) by displaying the resistivity and conductivity values. The film's conductivity rose from 1.711 to 2.423 (S/m) as its thickness decreased from 127.19 to 114.42 nm because of titanium concentration, resulting in a decrease in resistivity from 58.420 to 41.260 (Ω.cm). The electron-hole pairs in Tix MnNiO (X=1, 2, and 3 mL) are influenced by the titanium concentration, which is associated with the size of the crystals. The material's conductivity increases because of titanium concentration, which is attributed to the difference in crystallite sizes compared to MnNiO film. There is a correlation between the decrease in resistivity and film thickness of Tix MnNiO (X=1, 2, and 3 mL) and the concentration of titanium. These materials have the potential to improve solar cell efficiency. The resistivity of Tix MnNiO (X=1, 2, and 3 mL) makes it highly suitable for buffer layers in photovoltaic systems.

Table 2 Investigating the electrical characteristics of Tix MnNiO at different X values (1, 2, and 3 mL)

Films	t, (nm)	ρ, (Ω.cm) x 10^8	σ, (S/m) x 106
MnNiO	127.19	58.420	1.711
Ti $_{1\ mL}$MnNiO	121.97	52.941	1.888
Ti $_{2\ mL}$MnNiO	118.87	43.492	2.299
Ti $_{3\ mL}$MnNiO	114.42	41.260	2.423

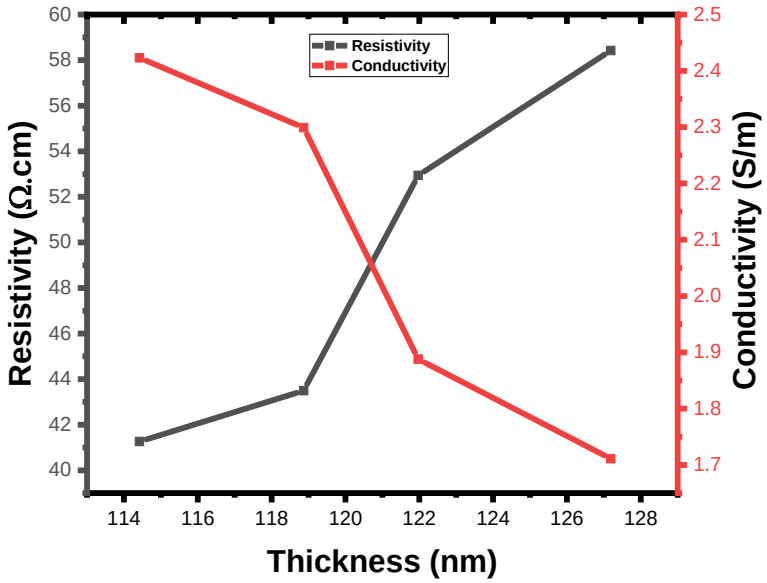

Figure 7 Resistivity and conductivity vs. thickness

Conclusion

Using a hydrothermal approach, we have successfully synthesized Tix MnNiO (X=1, 2, and 3 mL). The synthesized films are polycrystalline and exhibit a hexagonal phase. They show a preferred orientation along the (111), (112), (116), (121), and (200) planes. The 2 theta angles are (26.612, 30.816, 32.154, 33.154, and 37.856) degrees. Incorporating titanium into the lattice of manganese, nickel oxide improves the material's structural properties. The integration of titanium into the MnNiO lattice improved the material's UV absorbance. The prominent peaks of the materials are visible at 310 nm, suggesting an increase in titanium concentration during synthesis and enhancing material absorbance. As the wavelength of light in the visible region increases, the material's absorbance decreases. The indirect bandgap energy of the synthesized Tix MnNiO (X=1, 2, and 3 mL) film decreases as the molar concentration of the material increases, shifting from 2.75 eV to a range of 1.82-1.50 eV.

Conflict of interest

The authors declare that they have no personal or financial conflicts that could have influenced the research described in this article.

Availability of data

Upon request, data is available.

Acknowledgments

We extend our gratitude to all the authors for their contribution to the success of the research.

ORCID

Azmat Hussain
https://orcid.org/0000-0002-0426-5116
Saira Habib
https://orcid.org/0000-0002-8773-0609
Inam Ullah
https://orcid.org/0009-0001-4561-786X
Fahma Sahreen
https://orcid.org/0009-0006-6865-8492
Imtiaz Ahmad
https://orcid.org/0009-0003-7367-4188

Imosobomeh Lucky Ikhioya
https://orcid.org/0000-0002-5959-4427

References

[1]Josephine E. N., Ikponmwosa O. S., Ikhioya I. L., Enhanced physical properties of SnS/SnO semiconductor material, *Asian Journal of Nanoscience and Materials*, 2023, **3**:199 [Crossref], [Google Scholar], [Publisher]

[2]Ahmad I., Razzaq J., Ammara A., Kaleem F., Qamar M., Impact of Annealing Temperature on Hydrothermally Synthesized Copper Antimony Oxide (Cu_2Sb_2O) from Amorphous Phase to Monoclinic Structure, *Advanced Journal of Chemistry, Section A*, 2024, **7**:1 [Crossref], [Google Scholar], [Publisher]

[3]Ikhioya I. L. *et al.,* Impact of precursor temperature on physical properties of molybdenum doped nickel telluride metal chalcogenide material, *Asian Journal of Nanoscience and Materials*, 2023, **2**:156 [Crossref], [Google Scholar]

[4]Akaltun Y., Çayir T., Fabrication and characterization of NiO thin films prepared by SILAR method, *Journal of Alloys and Compounds*, 2015, **625**:144 [Crossref], [Google Scholar], [Publisher]

[5]Oliveira M.V.D.F., Delgado O.T., Cedro W.L., Rivera Y.R., Solovieva Y., Sant'anna G.L., Ribeiro A.L.C., Silva A.T.P.D., Moreira E.M.D.S.C., Coelho W.A.A., Rodrigues A.D.Q., Synthesis and characterization of nio for appications in photoelectronics devices, *ciência e engenharia de materiais: conceitos, fundamentos e aplicação*, 2021, **1**:374 [Crossref], [Google Scholar], [Publisher]

[6] Chukwuemeka E. J., Osita N. A., Odira A. O., Uchechukwu U. C., Mimi J. D., Ikhioya I. L., Performance and Stability Evaluation of Low-Cost Inorganic Methyl Ammonium Lead Iodide (CH3NH3PbI3) Perovskite Solar Cells Enhanced with Natural Dyes from Cashew and Mango Leaves, *Advanced Journal of Chemistry, Section A*, 2024, **7**:27 [Crossref], [Google Scholar], [Publisher]

[7]Shah H., Afzal S., Usman M., Shahzad K., Ikhioya I., Impact of annealing temperature on lanthanum erbium telluride (La0. 1Er0. 2Te0. 2) nanoparticles synthesized via hydrothermal approach, *J. Chem. A*, 2023, **6**:342. [Crossref], [Google Scholar], [Publisher]

[8] Udofia K.I., Ikhioya I.L., Okoli D.N., Ekpunobi A.J., Asian Journal of Nanoscience and Materials, *Asian Journal of Nanoscience and Materials*, 2023, **2**:135 [Crossref], [Google Scholar], [Publisher]

[9]Udofia K. I., Ikhioya I. L., Okoli D. N., Azubike J., Impact of doping on the physical properties of PbSe chalcogenide material for photovoltaic application, *Asian Journal of Nanoscience and Materials,* 2023, **2**:135 [Crossref], [Google Scholar]

[10] Sarwar S.G., Ikhioya I.L., Afzal S., Ahmad I., Supercapitance performance evaluation of MXene/Graphene/NiO composite electrode via in situ precipitation technique, *Hybrid Advances*, 2023, **4**:100105 [Crossref], [Google Scholar], [Publisher]

[11] Samuel S.O., Timothy Z.J., Ojoba C.K., Ikhioya I.L., Temperature's Impact on the Physical Properties of Rare Earth Element Doped SrS for Optoelectronic Use, 2023, **3**:147 [Crossref], [Google Scholar], [Publisher]

[12] Chen G.J., Lin C.M., Shih Y.H., Jian, S.R., The microstructures and characteristics of NiO films: Effects of substrate temperature, *Micromachines*, 2022, **13**:1940 [Crossref], [Google Scholar], [Publisher]

[13] da Silva A.K., Ricci T.G., de Toffoli A.L., Maciel E.V.S., Nazario C.E.D., Lanças F.M., The role of magnetic nanomaterials in

miniaturized sample preparation techniques, In *Handbook on Miniaturization in Analytical Chemistry* Elsevier, 2020, 77 [Crossref], [Google Scholar], [Publisher]

[14] Echresh A., Abbasi M.A., Shoushtari M.Z., Farbod M., Nur O., Willander M., Optimization and characterization of NiO thin film and the influence of thickness on the electrical properties of n-ZnO nanorods/p-NiO heterojunction, *Semiconductor Science and Technology*, 2014, **29**:115009 [Crossref], [Google Scholar], [Publisher]

[15] Garten L.M., Selvarasu P., Perkins J., Ginley D., Zakutayev A., Phase formation of manganese oxide thin films using pulsed laser deposition, *Materials Advances*, 2021, **2**:303 [Crossref], [Google Scholar], [Publisher]

[16] Indulal C.R., Biju R., Nand D., Raveendran R., Dielectric and Optical Band Gap Studies of Nanostructured Manganese Nickel Oxide and Cobalt Nickel Oxide, *Oriental Journal of Chemistry*, 2017, **33**:1581 [Crossref], [Google Scholar], [Publisher]

[17] Jadhav P.R., Shinde V.V., Navathe G.J., Karanjkar M.M., Patil P.S., June. Manganese oxide thin films deposited by SILAR method for supercapacitor application, In *AIP Conference Proceedings* American Institute of Physics, 2013, **1536**:679 [Crossref], [Google Scholar], [Publisher]

[18] Rajesh K., Pothukanuri N., Dasari S.G., Reddy M.R., Investigations of spray-deposited NiO thin films for ultrasensitive formaldehyde detection, *Journal of Alloys and Metallurgical Systems*, 2023, **2**:100009 [Crossref], [Google Scholar], [Publisher]

[19] Kumar N., Phani M.K., Chamoli P., Manoj M.K., Sharma A., Ahmed W., Srivastava A.K., Kumar S., Nanomaterials for advanced photovoltaic cells, *Emerging nanotechnologies for renewable energy*, 2021, 239 [Crossref], [Google Scholar], [Publisher]

[20] Maaoui B., Aoun Y., Benramache S., Nid A., Far R., Touati A., Synthesis and characterization of physical properties of the NiO thin films by various concentrations, *Advances in Materials Science*, 2020, **20**:79 [Crossref], [Google Scholar], [Publisher]

[21] Mane V.J., Malavekar D.B., Ubale S.B., Lokhande V.C., Lokhande C.D., Manganese dioxide thin films deposited by chemical bath and successive ionic layer adsorption and reaction deposition methods and their supercapacitive performance, *Inorganic Chemistry Communications*, 2020, **115**:107853 [Crossref], [Google Scholar], [Publisher]

[22] Napari M., Huq T.N., Hoye R.L., MacManus-Driscoll J.L., Nickel oxide thin films grown by chemical deposition techniques: Potential and challenges in next-generation rigid and flexible device applications, *InfoMat*, 2021, **3**: 536 [Crossref], [Google Scholar], [Publisher]

[23] Poulain R., Lumbeeck G., Hunka J., Proost J., Savolainen H., Idrissi H., Schryvers D., Gauquelin N., Klein A., Electronic and chemical properties of nickel oxide thin films and the intrinsic defects compensation mechanism, *ACS Applied Electronic Materials*, 2022, **4**: 2718 [Crossref], [Google Scholar], [Publisher]

[24] Ukoba K.O., Eloka-Eboka A.C., Inambao F.L., Review of nanostructured NiO thin film deposition using the spray pyrolysis technique, *Renewable and Sustainable Energy Reviews*, 2018, **82**: 2900 [Crossref], [Google Scholar], [Publisher]

[25] Xia H., Wan Y., Yan F., Lu L., Manganese oxide thin films prepared by pulsed laser deposition for thin film microbatteries, *Materials Chemistry and Physics*, 2014, **143**: 720 [Crossref], [Google Scholar], [Publisher]

[26] Yoshio M., Noguchi H., Secondary Batteries-Lithium Rechargeable Systems – Lithium-Ion | Positive Electrode: Manganese Oxides, *Encyclopedia of Electrochemical Power Sources*, 2009, 307 [Crossref], [Google Scholar], [Publisher]

[27] Zahan M., Podder J., Structural, optical and electrical properties of Cu: MnO_2 nanostructured thin films for glucose sensitivity measurements, *SN Applied Sciences*, 2020, **2**:1 [Crossref], [Google Scholar], [Publisher]

[28] Zankowski S.P., Van Hoecke L., Mattelaer F., De Raedt M., Richard O., Detavernier C., Vereecken P.M., Redox layer deposition of thin films of MnO_2 on nanostructured substrates from aqueous solutions, *Chemistry of Materials*, 2019, **31**: 4805 [Crossref], [Google Scholar], [Publisher]

[29] Zhang C., Zhang Y., Nie Z., Wu C., Gao T., Yang N., Yu Y., Cui Y., Gao Y., Liu W., Double Perovskite La_2MnNiO_6 as a High-Performance Anode for Lithium-Ion Batteries, *Advanced Science*, 2023, 2300506 [Crossref], [Google Scholar], [Publisher]

[30] Guo W., Yang T., Huang L., Wang S., Li, J., Hydrothermal preparation of $MnNiO_3/Ni_6MnO_8$ nanospheres on nickel foam as a high stability electrode material for supercapacitor, *Journal of Alloys and Compounds*, 2022, **924**: 166490 [Crossref], [Google Scholar], [Publisher]

[31] El Baakili S., Semlali A., El Mabrouk K., Bricha M., Synthesis Method Effect on Acellular Bioactivity of Bioglasses: Structural Analysis and Solid-State NMR, *Journal of Applied Organometallic Chemistry,* 2023, **3**:268 [Crossref], [Publisher]

[32] Ali F. *et al.,* Improved Morphological, Structural, and Optical Features of ErxCuNiO3 {x= 0, 0.5, 0.7, 0.9}, *Journal of Applied Organometallic Chemistry*, 2023, **3**:308 [Crossref], [Google Scholar], [Publisher]